View metadata, citation and similar papers at core.ac.uk

brought to you by CORE

provided by Online Research Database In Technology

Technical University of Denmark

Single-sided sheet-to-tube spot welding investigated by 3D numerical simulations

Nielsen, Chris Valentin; Chergui, Azeddine; Zhang, Wenqi

Publication date:
2012

Link back to DTU Orbit

Citation (APA):
Nielsen, C. V., Chergui, A., & Zhang, W. (2012). Single-sided sheet-to-tube spot welding investigated by 3D numerical simulations. Abstract from 7th International Seminar on Advances in Resistance Welding, Busan, Korea, Republic of.

DTU Library
Technical Information Center of Denmark

General rights
Copyright and moral rights for the publications made accessible in the public portal are retained by the authors and/or other copyright owners and it is a condition of accessing publications that users recognise and abide by the legal requirements associated with these rights.

- Users may download and print one copy of any publication from the public portal for the purpose of private study or research.
- You may not further distribute the material or use it for any profit-making activity or commercial gain
- You may freely distribute the URL identifying the publication in the public portal

If you believe that this document breaches copyright please contact us providing details, and we will remove access to the work immediately and investigate your claim.

Single-sided sheet-to-tube spot welding investigated by 3D numerical simulations

Chris Valentin Nielsen[1], Azeddine Chergui[2] and Wenqi Zhang[3]

[1]Manufacturing Engineering, Technical University of Denmark, cvni@mek.dtu.dk
[2]Dortmund FuE-A Pressfügen/Kleben, ThyssenKrupp, azeddine.chergui@thyssenkrupp.com
[3]SWANTEC Software and Engineering ApS, wz@swantec.com

Abstract

The single-sided resistance spot welding process is analyzed by a 3D numerical study of sheet-to-tube joining. Finite element simulations are carried out in SORPAS® 3D. Two levels of electrode force and five levels of welding current are simulated. The overall effects of changing current and force are discussed and special focus is put on the sensitivity to the electrode force and the potential of melt penetration to the inside of the tube. The electrode force is critical because the level is a compromise between sufficient contact area on one side and indentation and local deformation of the tube on the other side. The potential of melt penetration through the thickness of the tube during the hold time is a result of heat conduction in the tube material and lack of an electrode on the inside of the tube, which results in poor cooling of the inner tube surface.

1. INTRODUCTION

With intensive focus on weight and cost reductions in automobile manufacturing, it is becoming common to utilize hydroformed tubes as structural parts of the body-in-white as presented by Shah and Bruggemann [1]. The closed tubular shape provides sufficient stiffness with relative low weight compared to conventional stamped parts and is therefore attractive in vehicle design. The utilization of closed tubular parts, however, presents new challenges to the assembling procedures as e.g. discussed by Poss et al. [2] and Cho et al. [3]. The resistance spot welding process is the preferred joining technique in automotive assembly lines due to production cost and efficiency, versatility and robustness. The typical application of an electrode from each side of the weld is not feasible when spot welding sheet materials to closed tubular components. Single-sided spot welding is therefore utilized in order to facilitate welding of weld flanges or panels to the tubular structures.

In single-sided spot welding, a primary electrode is applied from the sheet side to impose the weld force and supply the weld current while a secondary electrode is introduced at another available location of the tube structure to supply electrical connection. This implies current flowing from the weld region to the secondary electrode with moderate heat generation as a result. Different locations may be utilized for the secondary electrode. In some cases it may be convenient to place it from the opposing side of the tube, while in other cases it may be more convenient to place it on the same side of the tube as the primary electrode.

The single-sided spot welding process is preferred prior to alternative welding techniques as presented by Cho et al. [3]. Arc welding is inducing larger thermal distortion and presenting quality control issues, and laser welding is expensive. Both alternative welding procedures may face problems in case of a gap between the sheet and tube because there is no applied force to bring the parts in proper contact.

A number of contributions [2-8] present experimental analysis of single-sided spot welding of sheet to tube combinations with squared or cylindrical cross-sections of the tube. The work by Rudolf [4] is accentuated as a thorough investigation of different weld parameters, welding positions, sheet and tube thickness ratios, and electrode shapes for squared and cylindrical cross-sectioned tubes with analysis of heat generation, contact development and deformation. Common for the experimental investigations by different authors is the narrow weldability lobes reported. The electrode force is critical in obtaining a proper weld. If the force is too low, splash is likely to occur between the sheet and the electrode, while if it is too large, the indentation is easily too big because of the absence of support on the inside of the tube. The local and global deformation is therefore largely depending on the stiffness of the tube as well as the degree of softening due to elevated temperatures. Large indentation can lead to torus shaped weld nuggets and cracks on the inside of the tube or in the sheet.

Numerical simulations based on finite element modeling are suited for assisting experimental investigations for further understanding and improvement of the process. Rudolf [4] presented numerical simulations performed in SORPAS®, which is dedicated to simulation and optimization of resistance welding (see e.g. [9]). At that time, SORPAS® was only available in 2D in terms of axisymmetric or block modeling. The work by Rudolf [4] concluded that the block model was not applicable for this geometry, while the axisymmetric model was able to provide useful information about the process. This is despite the fact that a sphere is actually simulated when modeling a cylindrical tube axisymmetric. Liang et al. [6,10] based their numerical analysis on ANSYS, but also with simplification to axisymmetric modeling.

With increasing insight into the process, the details that are sought for further understanding can only be simulated by 3D models that include the real geometry, facilitating the simulation of contact development, current density and heat development in three dimensions. This includes the asymmetries typically presented by the position of the secondary electrode resulting in asymmetric current flow, heat generation and softening.

Recent developments [11] have lead to the new finite element computer program SORPAS® 3D, which is specialized for simulation of resistance welding in three dimensions. This paper presents simulations from SORPAS® 3D of the single-sided spot welding process applied to sheet-to-tube joining together with an experimental setup from industry to enrich the presentation. The process is revisited by simulated effects that are only available by 3D simulations.

Analysis of the sheet-to-tube spot welding is an example of the applicability of SORPAS® 3D, while the availability leaves many other resistance welding cases to be further studied. Electrode misalignment, shunt effects and welding near edges are examples of spot welding including 3D effects. Projection welding is by nature relevant for 3D analysis due to the various geometries; square-nuts, hexagon-nuts and wires are typical examples among many possible geometries.

2. NUMERICAL MODELING

Numerical simulations are performed in the new computer program SORPAS® 3D, which is developed within the SORPAS® framework with the 3D thermo-mechanical engine shared with I-Form3 (see e.g. [12]), which is a thermo-mechanical forming program. SORPAS® 3D is currently in the stage of a beta-version as a complete standalone program including graphical interface, meshing facilities with hexahedral elements [11,13] and parallel computing [11,14] besides the core finite element module.

2.1. Coupled electro-thermo-mechanical finite element formulation

The core module consists of a coupled electro-thermo-mechanical finite element program. The mechanical model is responsible for deformation and stress distribution, while the electrical model is responsible for the distribution of the current density giving rise to heat generation by Joule heating. The temperature distribution and changes in material properties due to temperature are solved in the thermal model.

The mechanical model is based on the irreducible flow formulation, which in weak form suited for finite element implementation can be stated as follows,

$$\delta\Pi = \int_V \bar{\sigma}\delta\dot{\bar{\varepsilon}}dV + K\int_V \dot{\varepsilon}_V\delta\dot{\varepsilon}_V dV - \int_S t_i\delta u_i dS + \sum_{c=1}^{N_c} Pg_c\delta g_c \tag{1}$$

where δ indicates an arbitrary admissible variation in the velocity field, Π is the energy rate of the system, V is the domain volume with surface S, $\bar{\sigma}$ is the effective stress and $\dot{\bar{\varepsilon}}$ is the equivalent strain rate. The second term is to obey volume constancy in the plasticity formulation by penalizing the volumetric strain rate $\dot{\varepsilon}_V$ by a large positive constant K. The third term is eventual surface tractions t_i on surface with velocity u_i. Finally, the fourth term is for obeying mechanical contact between objects (workpieces, electrodes etc.) by penalizing normal velocity difference g_c in contact pair c (if otherwise resulting in penetration) by a large positive constant P. A contact pair consists of a node from one side of the contact and an element face of the other side (see details of the contact implementation elsewhere [11,15]).

The thermal model responsible for the temperature field T is governed by

$$kT_{,ii} + \dot{q} = \rho c\dot{T} \tag{2}$$

with thermal conductivity k, mass density ρ and heat capacity c. The heat generation is included by $\dot{q}$, which is the link to the electrical model generating heat according to Joule heating based on the electrical resistance and the current density (squared). The current density field is available from the gradient of the potential Φ governed in the electrical model by

$$\Phi_{,ii} = 0 \tag{3}$$

which in its form is identical to the stationary part of (2) because the transient part of the electrical field can be ignored compared to the transient response of the temperature field.

Contact resistance, being critical for the modeling of resistance welding, is evaluated based on the strength of the materials at the given temperature, the contact pressure and the electrical properties including restriction of the current and surface contamination in form of oxides, oils, films etc. [16-17].

2.2. Elastic effects

The irreducible flow formulation is a rigid-plastic formulation suited for large plastic deformations. In its original form, regions with less deformation (effective strain rate below a certain cutoff) are treated as rigid regions. In many resistance welding simulations, this

assumption is sufficient because only the local region around the weld is simulated. However, in the present study of sheet-to-tube spot welding, the global deformation of the tube is of importance for the local contact formation, and a larger amount of the real setup is therefore modeled. This implies that elastic effects are relevant for the present study because the global deformation of the tube is elastic.

Elastic effects are incorporated into the flow formulation based on the ideas presented by Mori et al. [18] and with details of the SORPAS® 3D implementation in [11]. In practical terms all elements are initialized as elastic elements following the constitutive law of elasticity until yielding. In the vicinity of the yield stress, the elements are changed into elasto-plastic elements and finally turned into rigid-plastic elements following equation (1) at stresses above the yield stress. A region around the weld zone will establish with rigid-plastic elements, the elements of the majority of the tube will be elastic, and the two regions are connected by elasto-plastic elements.

2.3. Material properties

SORPAS® 3D shares the material database with the 2D version, SORPAS®, already including all relevant material properties for the majority of typical steels and other metals welded by resistance welding.

3. WELD SETUP

An example of an experimental weld setup for the single-sided sheet-to-tube welding is provided in Figure 1. The tube is resting in a V-support while the sheet in positioned and welded from the top by applied force and current through the primary electrode. A flexible secondary electrode consisting of copper blades can be positioned arbitrarily on the tube with good electrical connection ensured by the mechanical flexibility.

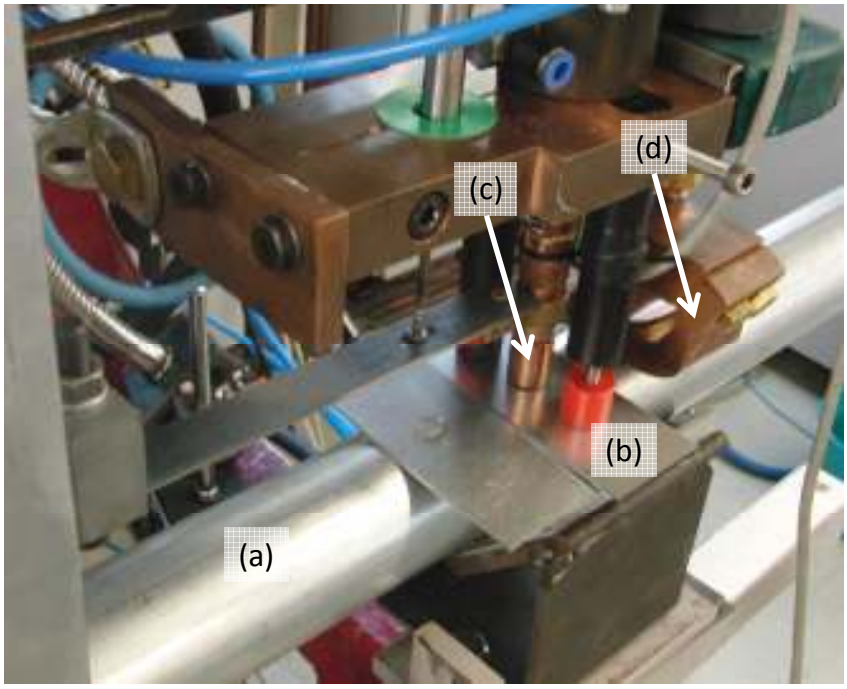

Figure 1: Experimental setup in laboratory of Dortmund FuE-A Pressfügen/Kleben, ThyssenKrupp for single-sided spot welding of sheet to tube consisting of (a) tube, (b) sheet, (c) primary electrode and (d) secondary electrode.

The primary electrode is controlled by a servo gun as suggested by Sun and Wang [19] that can supply a varying electrode force during the welding schedule. It is thereby possible to apply a larger electrode force in the early stage to ensure a mature contact condition between the sheet and the tube and to apply a lower electrode force in the later stage to avoid severe indentation due to softening of the sheet and tube without support on the inside.

Figure 2 shows an example of a spot weld obtained in the experimental setup. The cross-section in Figure 2a shows the indentation of the primary electrode into the sheet and corresponding local deflection of the tube. Figure 2b shows plug failure when tearing the sheet apart from the tube, which indicates a sound developed weld nugget.

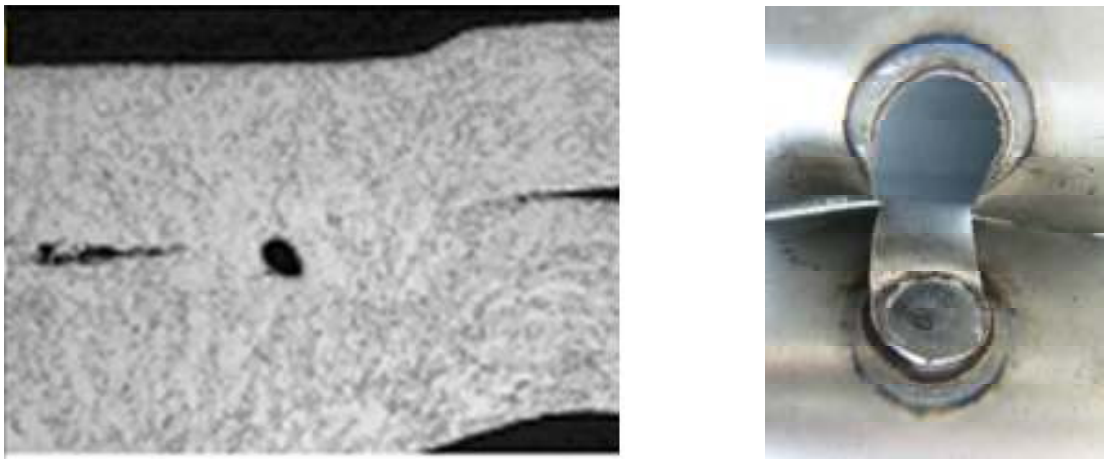

(a) *(b)*

Figure 2: Example of obtained weld by (a) cross-section of sheet (upper) and tube (lower) and (b) resulting plug failure upon separation.

4. SIMULATION SETUP

An example of single-sided sheet-to-tube spot welding is analyzed by numerical simulations. The example consists of a DP600 steel tube of inner diameter *52mm* and outer diameter *55mm*, such that the wall thickness is *1.5mm*. The sheet is *1mm* thick and made of DX54 steel. The primary electrode is modeled as *Ø16mm* F1-type with tip diameter *Ø5.5mm* and the secondary electrode is modeled as being placed *40mm* apart from the primary electrode center axis.

A section of the tube is cut out for analysis as shown in Figure 3a, where potential symmetry planes are also identified. The zx-plane is a pure symmetry plane, which is only violated if imperfections or misalignment is present. The yz-plane is more questionable because there is only a secondary electrode on one side (cf. Figure 1). If the asymmetries presented by this are of interest, the yz-plane cannot be utilized as a symmetry plane. However, in the present analysis, this effect is ignored and the focus is put on the contact development and heat development arising from the original line contact between the sheet and tube. Hence, the yz-plane is also utilized as a symmetry plane, and a finite element mesh as shown in Figure 3b is established when utilizing both symmetry planes. A third plane could be utilized as a symmetry plane; namely the plane parallel with the sheet cutting the tube into half. Experience from the simulations showed that the deformation field violated this symmetry condition due to local deformation propagating through the tube.

Figure 3b shows three tools supplying boundary conditions besides the two aforementioned symmetry planes. The top and bottom tools act as the connection to the machine from the electrode and the support on the underside of the tube. The third tool is specially developed for simulation of the secondary tool in an efficient and simple way. It is

specified as an electrical connection without mechanical influence to the simulation. This will simulate the good contact conditions resulting from the secondary electrode consisting of thin copper blades (see Figure 1). The deflection of the tube that can be caused by the secondary electrode is minimal and ignored by this tool.

The magnification in Figure 3b shows thin layers of elements on each side of the sheet to simulate the interfaces between the objects, especially the electrical contact resistance.

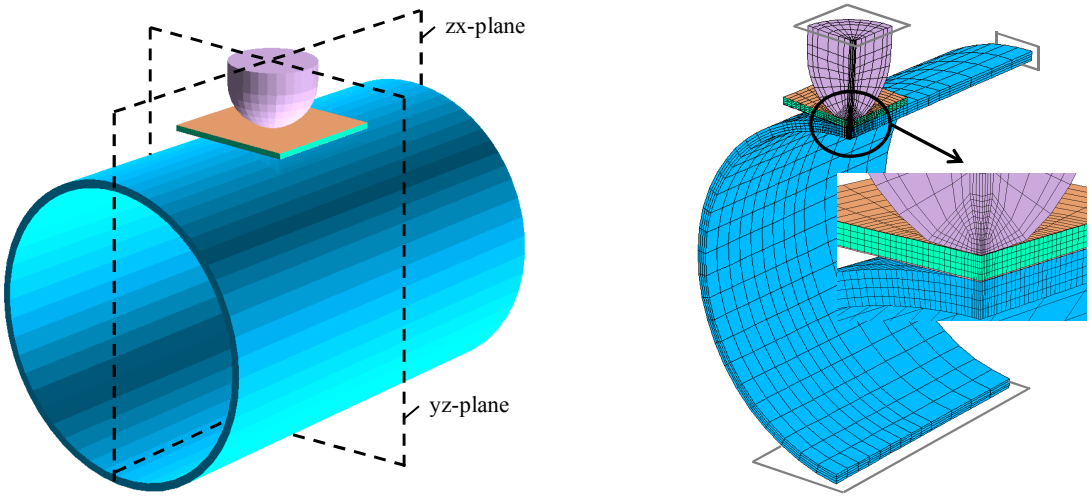

(a) *(b)*

Figure 3: Numerical model in terms of (a) identification of potential symmetry planes and (b) finite element mesh.

The individual meshes of the objects are shown in Figure 4 to present the details of the mesh allowing a reasonable discretization without a huge number of elements. The tube mesh is shown in Figure 4a with magnification of the mesh around the spot weld. The mesh is refined in this zone to be able to simulate the necessary gradients. Besides mesh refinement, the elements are aligned strategically such that they follow the overall shape of the weld zone and in particular the contact zone defined by the circular electrode tip. The circular alignment ensures smooth representation of the field variables, which would otherwise require many more elements.

The sheet mesh in Figure 4b follows the same strategy as the tube mesh. The electrode mesh is included in Figure 4c, where mesh refinement is also utilized. The two interfaces shown in the magnification in Figure 3b are not meshed independently, because they are automatically added in SORPAS® 3D after identification of relevant surfaces and specification of the layer thickness.

The welding process is analyzed for ten different weld settings, spanned by two force levels and five current levels while the process time is kept constant. The force and current profiles are illustrated in Figure 5. The force is raised to *1.5kN* or *1.8kN* before the current is applied. The current is applied with an up-slope of *60ms* to a level of *4*, *5*, *6*, *7* or *8kA* and then kept constant for additionally *140ms*. The force is constant during the up-slope current and then decreased during *30ms* to either *1.2kN* or *1.5kN*. The force is hereafter constant until the end of the hold time.

The electrode force of the primary electrode is assumed to be controlled by a servo gun such that the two levels can be used during one weld as suggested by Sun and Wang [19], and a DC current profile is assumed with the possibility of using an up-slope. The higher level of the force in the early stage of welding is, together with the up-slope of the current, prescribed in order to ensure a mature contact area before reaching the full current level. The applied

force is then lowered in the later stage of welding in order to decrease the indentation and local deformation due to softening an lack of support on the inside of the tube.

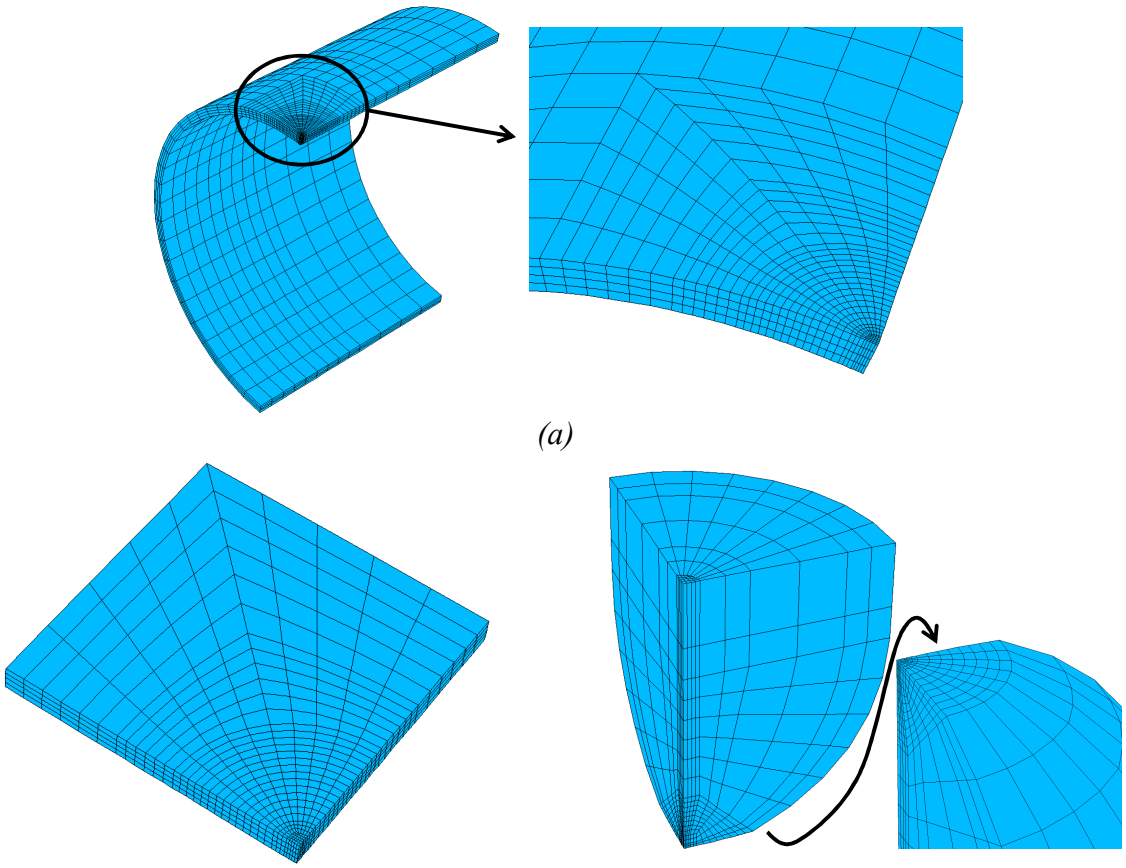

(a)

(b) *(c)*

Figure 4: Object mesh of (a) tube, (b) sheet and (c) primary electrode.

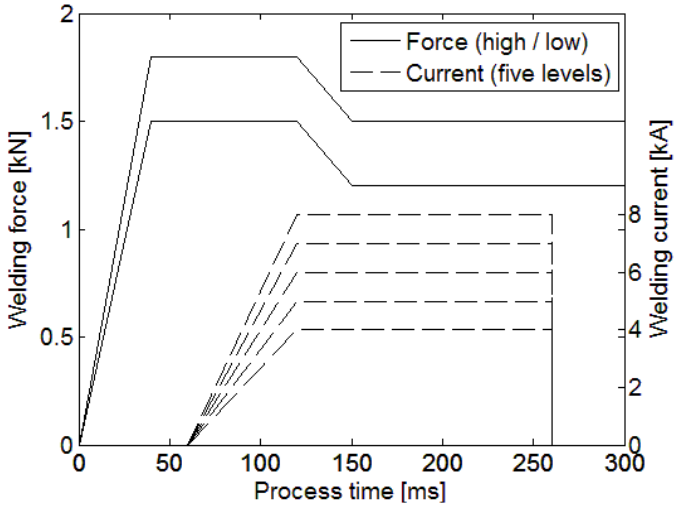

Figure 5: Two selected electrode force levels and five selected current levels. All ten combinations are simulated.

5. RESULTS AND DISCUSSION

Simulations with the ten different weld settings are presented in Figure 6 by the process peak temperature in the end of the weld time, i.e. at process time *260ms* in Figure 5, where the current is switched off. Each subfigure in Figure 6 shows the resulting peak temperature field in a view similar to that utilized in Figure 3b, and they are organized such that the left column contains the welds performed at the low force level (see Figure 5) and the right column contains the welds performed at the high force level. Each row corresponds to one level of the current as specified in the left side of the figure.

At both force levels it is clear that the weld nugget increase in size with increasing current and eventually penetrates through the tube to melt through. At the low force level, this happens already between *6kA* and *7kA*, while at increased force level it is postponed to between *7kA* and *8kA*. As it will be discussed ahead, it is also necessary to examine the subsequent cooling time for the evaluation of melting through to the inside of the tube because lack of an electrode on the inside of the tube results in poor cooling on the inner tube surface.

Figure 6 shows that the weld nuggets resulting from a higher force level are smaller than the similar welds resulting from lower force level, which is to be expected due to larger and better contact obtained at the higher electrode force. Larger indentation and local deformation can be expected as a consequence of the high force, but this is partly compensated by less softening due to smaller heat generation. Increased indentation and local deformation is therefore not considered to be a problem when going from the low to the high force level in Figure 5. However, this conclusion is closely related to a moderate increase in the force (20% in the early stage and 25% in the later stage).

From Figure 6 it appears that the higher force level in the present study results in better weld quality than the lower force level because of the increased contact area. Figure 7 exemplifies this for the cases with *6kA* weld current, which seems to present mature weld nuggets. Because the contact area in the early stages is smaller with the low electrode force (Figure 7a), the heat generation is more intense and the nugget height and risk of penetration through the tube are larger than with the high electrode force level (Figure 7b). The smaller contact area in the later stages combined with the larger weld nugget result in increased risk of splash between the sheet and the tube near the gap resulting from the curvature of the tube. The solid load bearing area that encloses the liquid in order to avoid splash is marked in both of the cases in Figure 7. The comparison reveals that at low force (Figure 7a), the nugget is larger while the contact area is smaller, and therefore this weld setting has higher risk of splash.

Spot welding the sheet to the tube by the high electrode force setting with a current level of *6kA* seems from Figure 6f and Figure 7b to result in a well-shaped nugget of a proper size while sufficient contact area is formed to avoid splash. It is nevertheless necessary to consider the cooling of the spot weld as unveiled above. The hold time ensures that a spot weld solidifies and get enough strength before the electrode force is released and the electrode moved. The electrodes absorb the majority of the heat and lead it away due to high thermal conductivity. However, in the single-sided spot welding there is no electrode on the inside of the tube and hence poor cooling on this side. The resulting cooling process during the hold time is depicted in Figure 8 for the case with *6kA* weld current and high electrode force. The sequence of depicted temperature fields starts from the end of the weld time and goes into the hold time in steps of *30ms*.

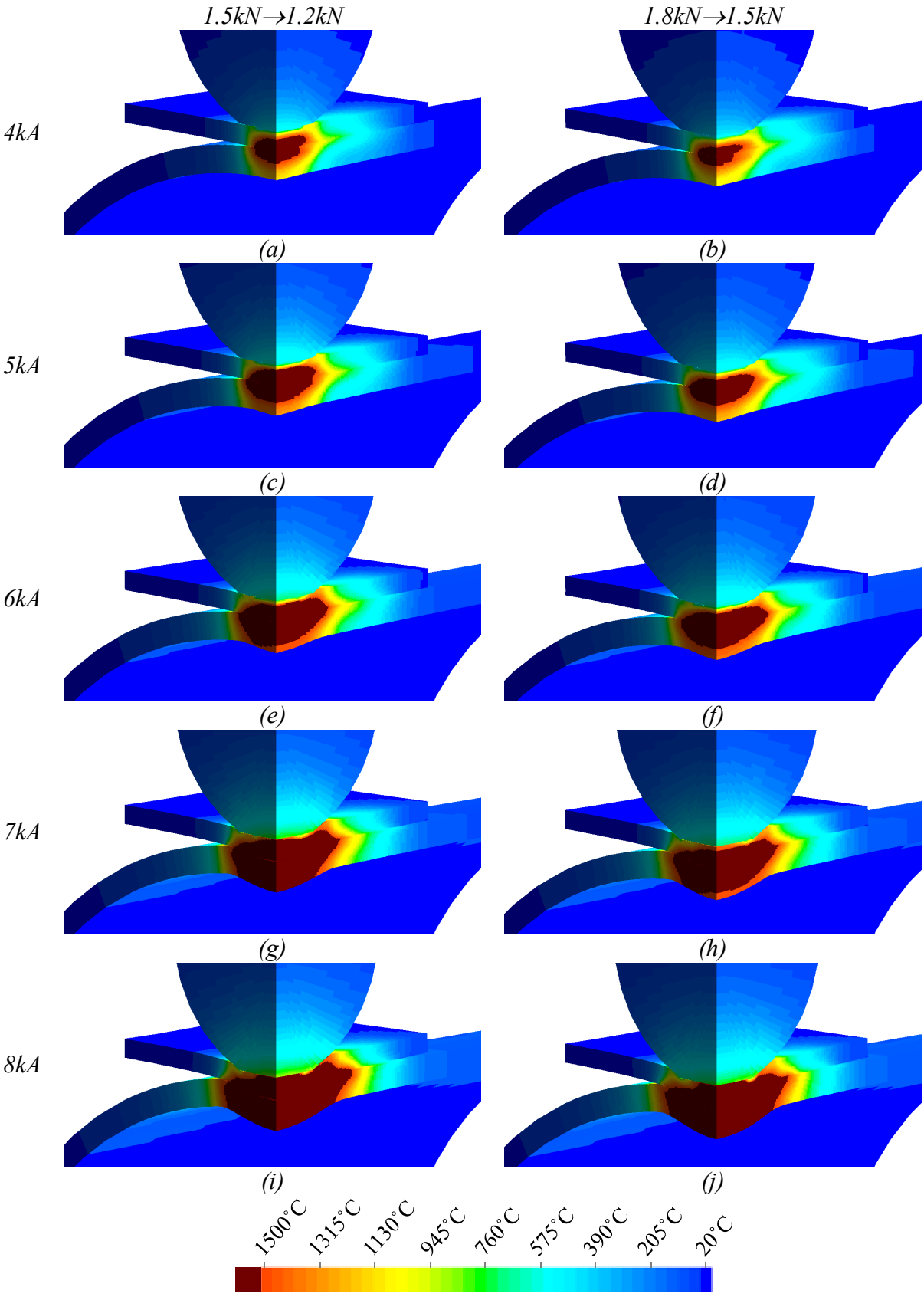

Figure 6: Process peak temperatures in the end of the weld time for different weld settings. The force and current profiles follow Figure 5. Force levels are indicated above the columns and current levels are indicated in the left side.

The sequence of temperature fields shows that the overall temperature naturally decreases, but it also shows that the temperature initially penetrates through the tube thickness as a result of heat conduction in the tube and poor cooling on the inner surface. The third temperature field, corresponding to *60ms* into the hold time, shows the penetration through the tube thickness to the inner surface. The two last temperature fields, corresponding to *180ms* and *210ms* into the hold time, are after complete solidification of the weld nugget. The solidification at the original interface position of the two materials take place in between the fourth and the fifth depicted time instants, i.e. between *120ms* and *150ms* into the hold time.

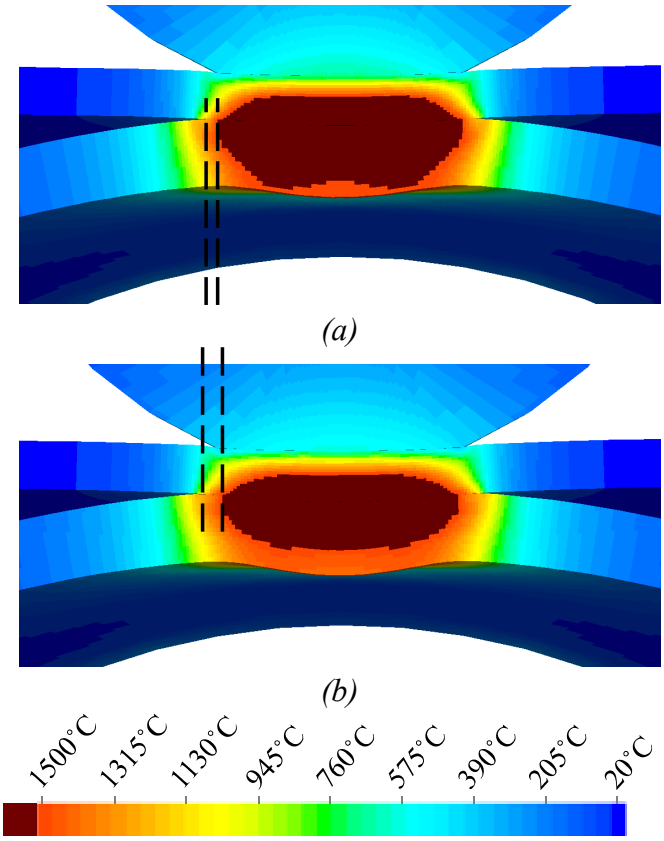

Figure 7: Comparison of cross-sections (corresponding to the yz-plane in Figure 3a) with process peak temperatures shown for the cases with 6kA current level and (a) low force level and (b) high force level.

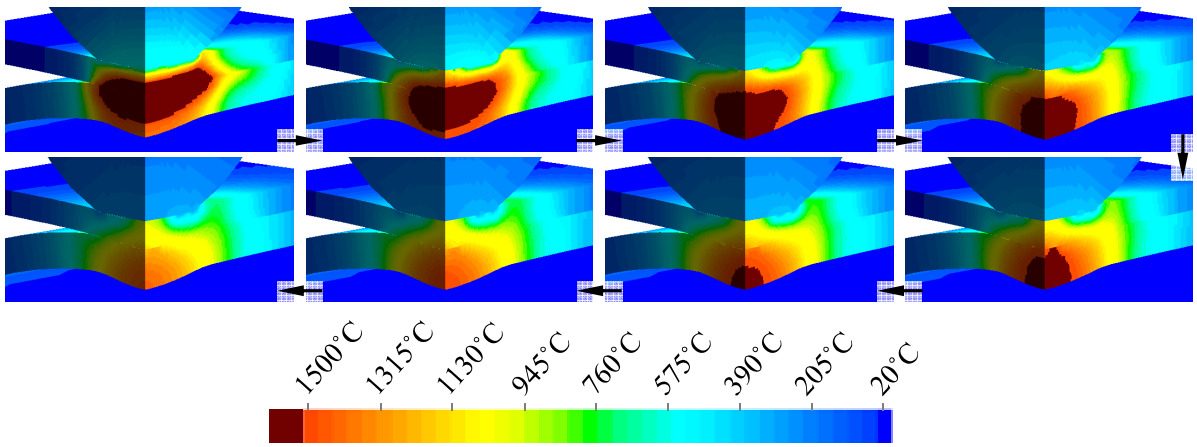

Figure 8: Temperature during the hold time for the case with 6kA and high force. The upper left subfigure corresponds to the end of the weld time. Following the arrows, each subfigure corresponds to additional 30ms into the hold time.

6. CONCLUSIONS

A 3D numerical study has been presented for an industrial resistance welding case in form of single-sided spot welding of a sheet to a tube, which is common when hydroformed tubular parts are included as structural parts in automotives to save weight. A number of weld settings are simulated to show the influence of changing parameters. Two levels of electrode force and five current levels are simulated with constant process time.

Besides selection of current level for the heat generation, it is shown and discussed how the electrode force influences the weld quality. A sufficient force is required for establishing an initial contact area large enough to stand the applied welding current, but on the other hand a too large force would result in excessive indentation and local deformation in the tube. A certain amount of indentation is though needed because this is allowing the sheet and tube in the later weld stage to be in contact over an area large enough contain the weld nugget and avoid splash.

The numerical study was also used to highlight the importance of the cooling during the hold time. Since there is no electrode on the inside of the tube, the weld nugget has potential of penetrating through the tube thickness to the inside surface. This is accommodated by heat conduction in the tube material while the lack of an inner electrode presents poor cooling on this side.

The present study, which is the only 3D numerical study of the single-sided sheet-to-tube welding that the authors are aware of, is providing simulations of the real process by taking into account the actual contact area formed between the sheet and the tube. The sheet is initially contacting the tube along a line, and the deformation caused by the electrode force develops the contact area dynamically in three dimensions during the welding process.

Besides future comparisons with corresponding experiments with specific welding parameters, it is of interest to simulate the effect of the position of the secondary electrode. The secondary electrode presents asymmetry which was neglected in the present study, but a future study could involve these effects.

The existence of the new computer program, SORPAS® 3D, provides the ability of simulating a variety of resistance welding cases that is not properly simulated by 2D analysis. As already mentioned in the end of the introduction, this includes electrode misalignment, shunt effects and welding near edges as regards spot welding, while projection welding in many cases is relevant for 3D analysis because the geometries cannot be simplified to 2D. Among geometries that are naturally simulated in 3D are square-nuts, hexagon-nuts, wires, longitudinal embossments and components with multiple projections.

References

[1] S. Shah and C. Bruggemann: “Tube hydroforming – process capability and production applications”, *Proceedings of International Body Engineering Conference IBEC ‘94,* Detroit, Michigan, 1994. pp. 26-30.

[2] M.G. Poss and J.M. Lendway IV: “Closed tubular automobile parts demand innovative welding methods”, *Welding Journal 76(10)*, 1997. pp. 55-58.

[3] Y. Cho, I. Chang, and H. Lee: “Single-sided resistance spot welding for auto body assembly”, *Welding Journal 85(8)*, 1997. pp. 26-29.

[4] H. Rudolf: *Widerstandspunktschweissen von Blech-Hohlprofil-Verbindungen an verzinkten Stahlblechen*, Dr.-Ing. Dissertation, TUDpress, Dresden, 2007.

[5] HG. Yang: “Investigations on sheet to cylindrical tube single-sided spot welding using servo gun”, *2010 International Conference on Computer, Mechatronics, Control and Electronic Engineering (CMCE),* 2010. pp. 256-258.

[6] C. Liang, F. Sun, and X. Liu: "Effect of weld parameters on weld quality in sheet to tube joining with simulation and experimental research", *2011 International Conference on Consumer Electronics, Communications and Networks (CECNet),* 2011. pp. 302-305.

[7] H.G. Yang, S.J. Hu, Y.S. Zhang, Y.B. Li, and X.M. Lai: "Experimental study of single sided sheet to tube resistance spot welding", *Science and Technology of Welding and Joining 12(6)*, 2007. pp. 530-535.

[8] Y.B. Li, C.P. Liang, Y.S. Zhang, and Z.Q. Lin: "Application of electrode force change in single sided resistance spot welding using servo gun", *Science and Technology of Welding and Joining 13(7)*, 2008. pp. 671-678.

[9] W. Zhang: "Weld planning with optimal welding parameters by computer simulations and optimizations", *Proceedings of The 6th International Seminar on Advances in Resistance Welding,* Hamburg, Germany, 2010. pp. 119-127.

[10] C.-P. Liang, Z.-Q. Lin, G.-L. Chen, and Y.-B. Li: "Numerical analysis of single sided spot welding process used in sheet to tube joining", *Science and Technology of Welding and Joining 11(5),* 2006. pp. 609-617.

[11] C.V. Nielsen, W. Zhang, L.M. Alves, N. Bay, and P.A.F. Martins: *Modeling of Thermo-Electro-Mechanical Manufacturing Processes: Applications in Metal Forming and Resistance Welding,* Springer, To be published.

[12] M.L. Alves, J.M.C. Rodrigues, and P.A.F. Martins: "Simulation of three-dimensional bulk forming processes by finite element flow formulation", *Modelling and Simulation in Materials and Engineering – Institute of Physics 11*, 2003. pp. 803-821.

[13] C.V. Nielsen, J.L.M. Fernandes, and P.A.F. Martins: "All-hexahedral meshing and remeshing for multi-object manufacturing applications", *Submitted for publication in international journal.*

[14] C.V. Nielsen and P.A.F. Martins: "Parallel skyline solver: Implementation for shared memory on standard personal computers", *Submitted for publication in international journal.*

[15] C.V. Nielsen, P.A.F. Martins, W. Zhang, and N. Bay: "Mechanical contact experiments and simulations", *Steel Research International 82*, 2011. pp. 645-650.

[16] W. Zhang and L. Kristensen: "Finite element modeling of resistance spot and projection welding processes", *The 9th International Conference on Computer Technology in Welding*, 1999. pp. 15-23.

[17] W. Zhang: "Design and implementation of software for resistance welding process simulations", *Transactions: Journal of Materials and Manufacturing 112(5)*, 2003. pp. 556-564.

[18] K. Mori, C.C. Wang, and K. Osakada: "Inclusion of elastic deformation in rigid-plastic finite element analysis", *International Journal of Mechanical Sciences 38*, 1996. pp. 621-631.

[19] P.C. Sun and P.C. Wang: "Sheet-to-tube resistance spot welding using servo gun", *US patent no. 7,060,929 B2*, 2006.